Electronic Supplementary Material (ESI) for Materials Chemistry Frontiers.

Supporting Information

Composite Clusters: $Co_{5.7}Ni_{2.3}W_{12}O_{42}(OH)_4$@Fluoro-Graphdiyne as a Stable Electrode for Sustained Electrochemical Oxygen Evolution at High Current Conditions

Hao Sun,[a] Xiaomei Xu,[a] Chaojun Jing,*[a] Wenhui Shang,[a] Yongchun Wang,[a] Muling Zeng,*[b] Zhiyu Jia*[a]

[a] MOE Key Laboratroy of Cluster Science, Beijing Key Laboratory of Photoelectronic/Electrophotonic Conversion Materials, School of Chemistry and Chemical Engineering, Beijing Institute of Technology, Beijing 100081, P. R. China.

[b] School of Biotechnology and Health Sciences, Wuyi University, Jiangmen, 529020, P. R. China.

E-mail address: jzy@bit.edu.cn (Z. Jia), jingcj@bit.edu.cn, (C. Jing), mulingzeng@163.com (M. Zeng)

Materials and Methods.

Reagents. All commerically acquired reagents were used as received. Dichloromethane and diethyl ether were used as received. Tetrahydrofuran was dried by passing through a column of activated molecular sieves using a solvent purification system. All water used was purified with a Millipore system (typically 18.2 MΩ cm resistivity).

Reaction conditions. Reaction requiring inert atmosphere was conducted under nitrogen using standard Schlenk line techniques. All other reactions were performed employing standard organic synthesis protocols.

Chromatography. Thin layer chromatography (TLC) was performed using Merck aluminium-backed plates of TLC Silica gel 60 F_{254}; the plates were revealed using UV light. Standard Flash Column chromatography was accomplished using silica gel (60 Å pore size, 230-400 µm mesh size).

NMR. Spectra were recorded using Bruker Avance 400 spectrometers (Analysis & Testing Center, Beijing Institute of Technology).

Turnover frequency (TOF). The turnover frequency (TOF) was determined to better explore the intrinsic activity of the $Ni_{5.7}Co_{2.3}$-POM@FGDY/NF and $Ni_{5.7}Co_{2.3}$-POM/NF in the OER by using the approach of redox peak integration of CV in static solution, which was calculated from the expression:

$$TOF = \frac{j \times S}{2Q_{redox}}$$

(where j is current density at a certain overpotential, S is the area of nanocomposite electrode and Q_{redox} is the transferred charges when redox reaction occurs at the active sites).

Synthesis of $Co_{5.7}Ni_{2.3}$-POM@FGDY composite cluster.

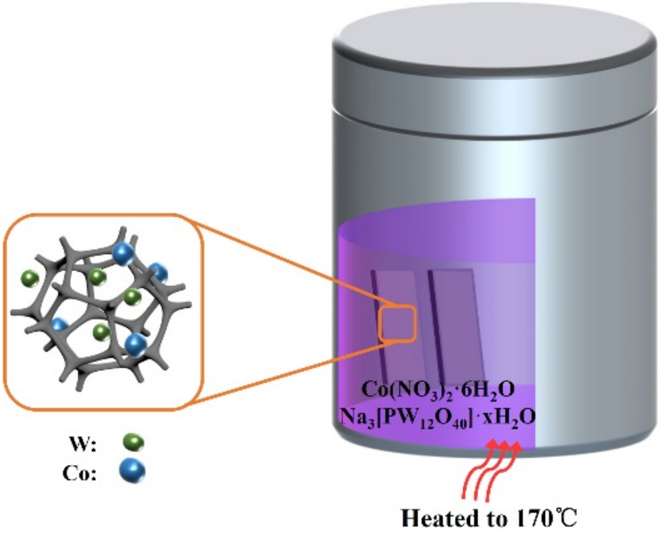

Fig. S1. Illustration of the hydrothermal reaction for $Co_{5.7}Ni_{2.3}$-POM.

1. Optimization of CoNi-POM cluster

$Co(NO_3)_2 \cdot 6H_2O$ (0.125 mmol) and $Na_3[PW_{12}O_{40}] \cdot xH_2O$ (0.125 mmol) were mixed in deionized H_2O (10 mL) in a 25 mL Teflon autoclave for 2 hours, and then the solution was adjusted pH to 2.0, 3.0, 4.0, 5.0, 6.0, 7.0 by HCl. Teflon autoclave was heated to 170 °C for 8 h (Figure S2).

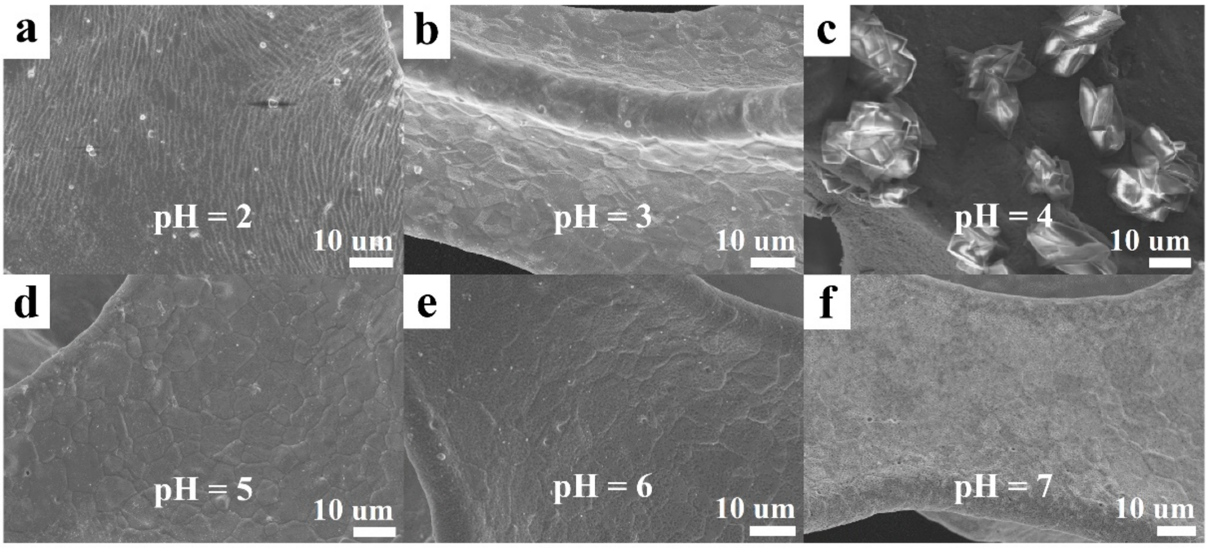

Fig. S2. The SEM of CoNi-POM electrode at different pH condition.

2. Synthesis of 1,3,5-(trimethylsilyl)ethynyl-2,4,6-trifluorobenzene

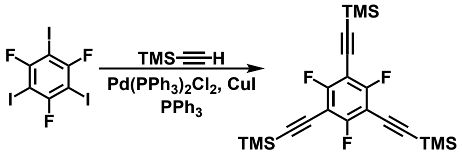

A solution of 1,3,5-trifluoro-2,4,6-triiodobenzene (2 mmol, 1.01 g), [Pd $(PPh_3)_2Cl_2$] (0.04 mmol, 28 mg), and CuI (0.08 mmol, 15.2 mg) and PPh_3 (0.08 mmol, 21 mg) in a mixture of THF (15 mL) and Triethylamine (15 mL) was allowed to stir in a closed flask (under N_2). A solution of ethynyltrimethylsilane (8 mmol, 786 mg, 1.13 mL) was added to above solution. The mixture was heated at 80 °C for 12 h. The mixture was quenched with water (2 mL) and was transferred to a separatory funnel. The organic layer was separated and the aqueous was extracted with dichloromethane (3 × 20 mL). The combined organic fraction was dried over Na_2SO_4 and the concentrated to dryness. The crude product was purified by flash chromatography. Flash column chromatography: silica gel, Hexane ($R_f = 0.4$). White solid, 446 mg, yield: 53%. ^1H NMR (400 MHz, $CDCl_3$) δ 0.26 (s, 27H). ^{13}C NMR (100 MHz, $CDCl_3$) δ 164.45 (C-F), 161.84 (C-F), 106.89 (C-Si), 99.69 (Ar), 88.74 (C≡C), 0.23 (CH_3). HRMS (ESI) m/z calcd for $C_{21}H_{27}F_3Si_3$ 420.1373, found: 420.1369.

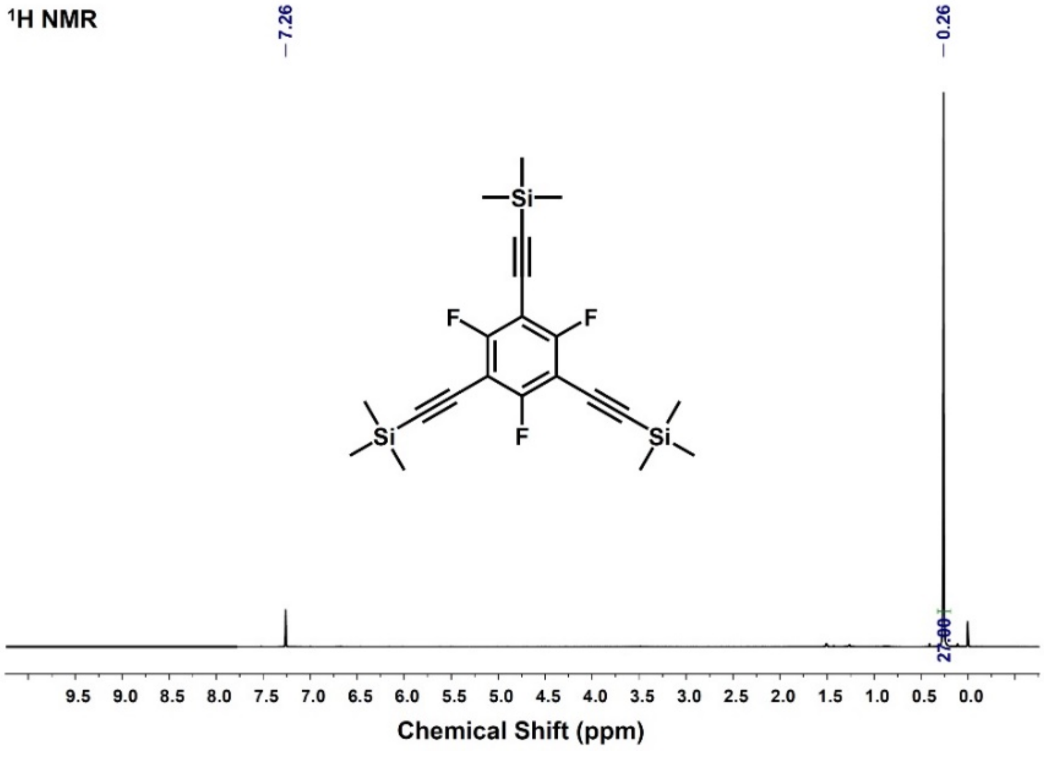

Fig. S3. ^{1}H NMR of 1,3,5-(trimethylsilyl)ethynyl-2,4,6-trifluorobenzene.

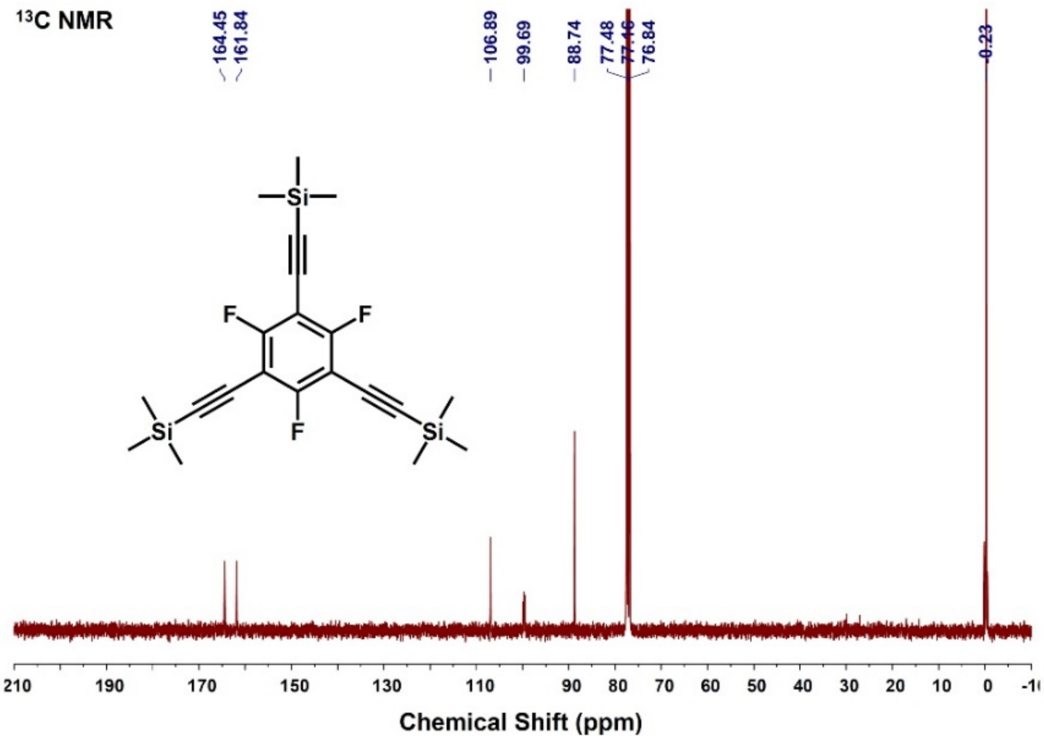

Fig. S4. ^{13}C NMR of 1,3,5-(trimethylsilyl)ethynyl-2,4,6-trifluorobenzene.

3. Synthesis of 1,3,5-triethynyl-2,4,6-trifluorobenzene.

1,3,5-(trimethylsilyl)ethynyl-2,4,6-trifluorobenzene (40 mg) was added to THF (10 mL), and then excessive TBAF was added to above solution for 15 min. The reaction was test by TLC, the starting substrate was disappeared at this point. And the reaction was quenched by Water (5 mL), ethyl acetate (EtOAc, 10 mL) was added to the reaction system. The mixture was washed with saturated aqueous NaCl, then evaporated to dryness. Because 1,3,5-triethynyl-2,4,6-trifluorobenzene is modestly stable in solvent at room temperature, the solvent was evaporated under vacuum at 30°C, and then EtOAc (5 mL) was added under nitrogen atmosphere at 0°C. The primrose yellow solution is used for the fabrication of $Co_{5.7}Ni_{2.3}$-POM@FGDY electrode.

4. Bulk Synthesis of FGDY powder.

After the successful synthesis of $Co_{5.7}Ni_{2.3}$-POM@FGDY electrodes, we have utilized 1,3,5-triethynyl-2,4,6-trifluorobenzene to synthesize FGDY powder in bulk. Copper foil (1 cm × 1 cm, 4 pieces) were added to the above mixed solution of EtOAc (80 mL), pyridine (8 mL). 1,3,5-triethynyl-2,4,6-trifluorobenzene (40 mg) was dissolved in 40 mL of EtOAc and added into the reaction mixture mentioned above. Then the reaction mixture was constantly stirred at 50 °C under a Ar atmosphere for 2 days. The reaction flask was covered with Al foil to protect it from light. After completion of the reaction, the crude product was removed from copper foil, and washed with acetone and water. The washed crude product was added slowly to 20 mL of hydrochloric acid (6 M). This was followed by dilution with water and subsequent filtration to obtain the pure product (19 mg). The FGDY powder was used for XPS test.

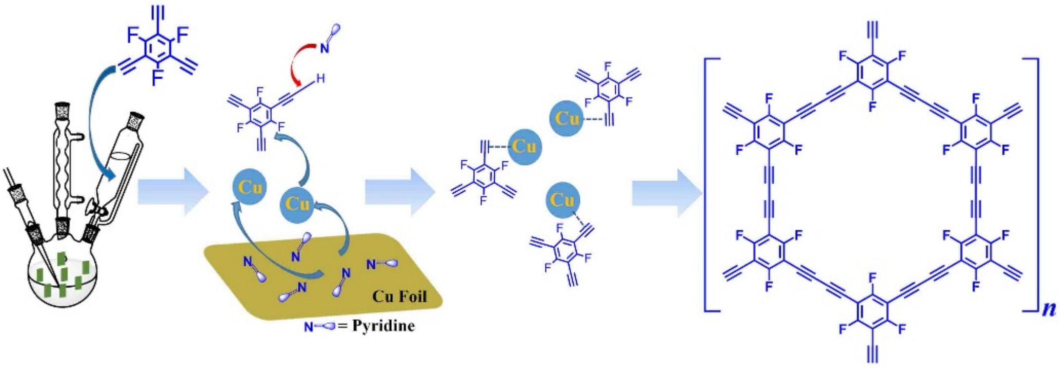

Fig. S5. Schematic of large-scale FGDY synthesis.

Characterization of $Co_{5.7}Ni_{2.3}$-POM@FGDY.

5. Inductively Coupled Plasma Optical Emission Spectrometer

Element analysis (ICP-OES, wt.-%) for a dried CoNi-POM microcrystal sample (removed mechanically from the Ni foam): Co 1.05 %, Ni 0.41 %.

6. Thermal properties

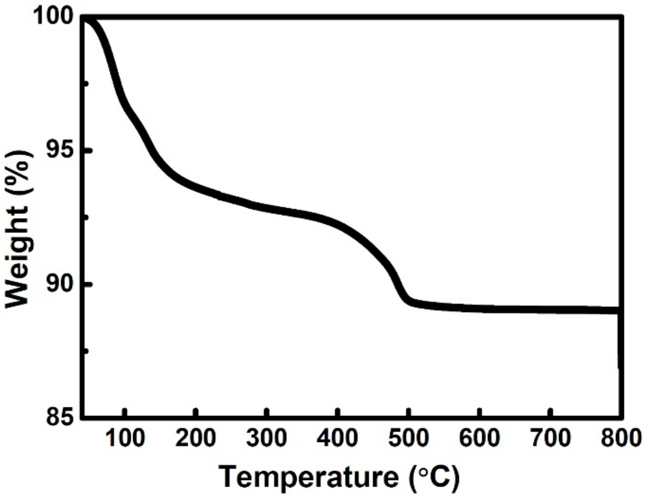

Fig. S6. TGA-DSC curves of $Co_{5.7}Ni_{2.3}$-POM.

Due to the removal of water molecules and hydroxyl groups, the weight loss of $Co_{5.7}Ni_{2.3}$-POM is 2.1% and 8.2%, respectively. From the thermogravimetric curve, we can calculate the real hydroxyl group and water molecules is about 4 and 16, to determine the final chemical formula: $Co_{5.7}Ni_{2.3}W_{12}O_{42}(OH)_4(H_2O)_{16}$.

7. X-ray photoelectron spectroscopy (XPS)

7.1 X-ray photoelectron spectroscopy (XPS) of $Co_{5.7}Ni_{2.3}$-POM

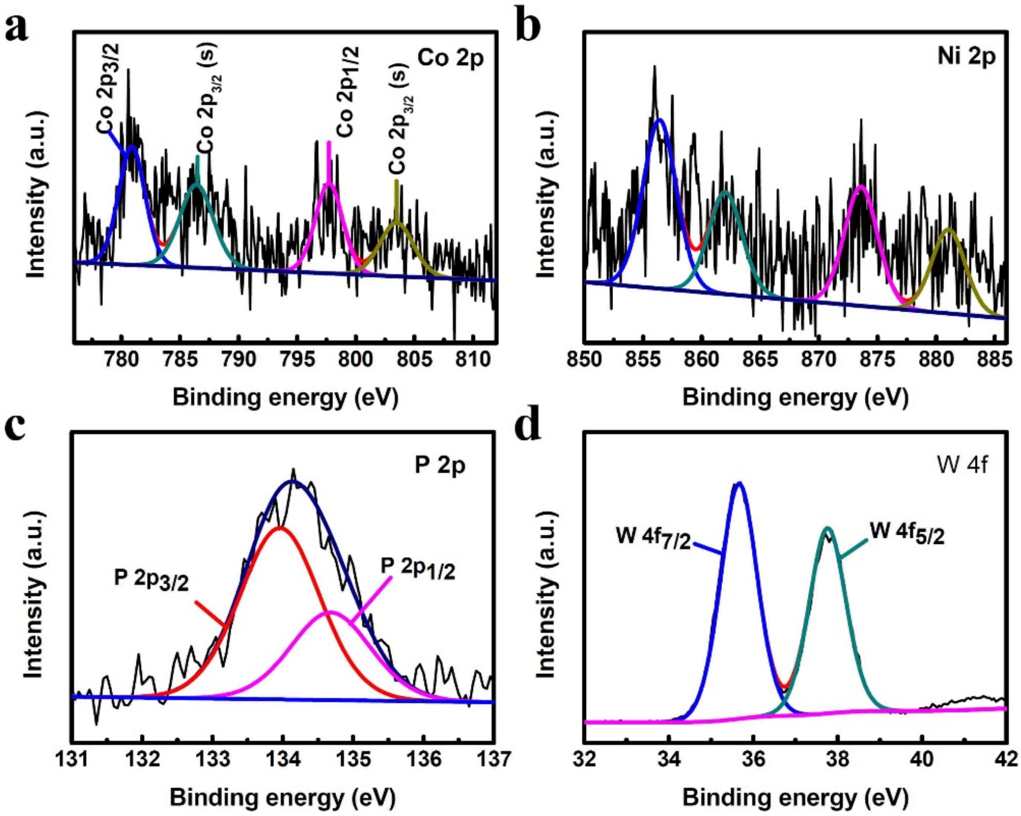

Fig. S7. The high-resolution XPS spectra of $Co_{5.7}Ni_{2.3}$-POM showing the (a) Co 2p; (b) Ni 2p; (c) P 2p; (d) W 4f.

For $Co_{5.7}Ni_{2.3}$-POM, The Co 2p spectra (Fig. S7a) presented two main peaks at ≈ 780.9 ($2p_{3/2}$) and ≈ 797.7 eV ($2p_{1/2}$). The satellite peaks of 2p Co^{2+} can also be observed at ≈ 6 eV, which is higher than those for $2p_{3/2}$ and $2p_{1/2}$. There are four peaks could be found for Ni 2p signal in the binding energy range of 855-884 eV (Fig. S7b), the main Ni $2p_{3/2}$ peak at 856.4 eV and its satellite at 862.0 eV, and the Ni $2p_{1/2}$ main peak and its satellite at 875.7 eV and 881.0 eV, respectively. The P 2p high-resolution spectra of $Co_{5.7}Ni_{2.3}$-POM was shown in Fig. S7c, and the binding energies of P 2p can be resolved into $2p_{3/2}$ and $2p_{1/2}$ doublets. All the spectra were fitted with one pair of peaks with 2p3/2 at binding energies close to 134 eV and 2p1/2 at ≈135 eV. For W 4f (Fig. S7d), the binding energies are resolved into $4f_{7/2}$ and $4f_{5/2}$

doublets induced by spin−orbital coupling. All W 4f spectra were fitted with one pair of peaks with $4f_{7/2}$ at binding energies close to 36 eV and $4f_{5/2}$ at ≈ 38 eV.

7.2 X-ray photoelectron spectroscopy (XPS) of FGDY

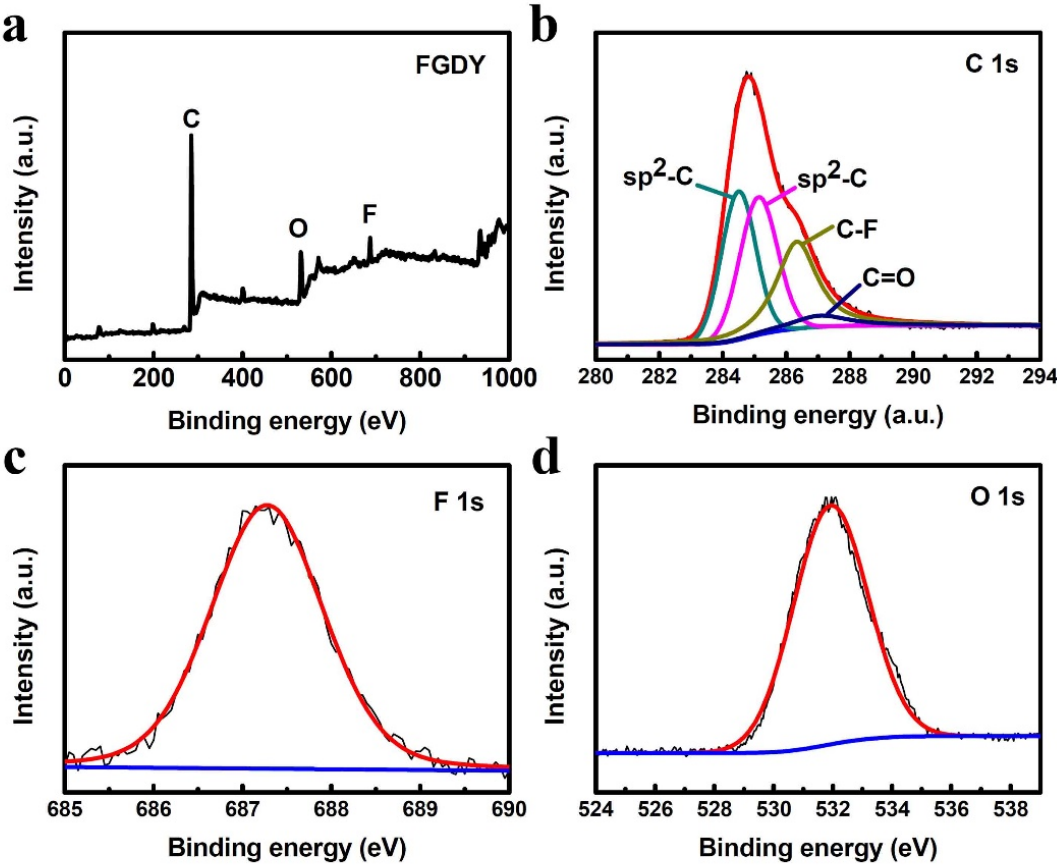

Fig. S8. (a) XPS survey spectrum of FGDY; (b) high-resolution XPS spectra of FGDY showing the (b) C 1s, (c) F 1s, (d) O 1s.

As shown in Fig. S8a, the XPS survey scan of FGDY exhibited that it is composed of C (1s), F (1s) and O (1s). The XPS C 1s spectrum in Fig. S8b shows peak at 284.8 eV which can be deconvolved into four peaks, corresponding to sp^2 (C=C) at binding energy of 284.5 eV, sp (C≡C) at 285.2 eV, C-F at 286.3 eV and C=O at 288.0 eV respectively. The integrated peak area ratio of sp^2-C versus sp-C is 1.0, in accordance with the chemical composition of FGDY. As shown in Fig. S8c, the fluorine peak at 687.3 eV could attribute to the semi-ionic C-F bond with high polarity, which would enhance the catalytic activity. The XPS O 1s spectrum shows that the p-FGDY sample has only one peak centered at 532.5 eV (Fig. S8d), which due to the absorption of air in FGDY.[1] These above results indicate that we had synthesized FGDY successfully.

Electrochemical of $Co_{5.7}Ni_{2.3}$-POM@FGDY electrode.

8. Detailed Calculation of EASA.

The electrochemically active surface area (EASA) value was estimated from the electrochemical double-layer capacitance (C_{dl}) of the catalyst. C_{dl} was measured via cyclic voltammograms with a potential range where no apparent Faradaic process was taking place. The double-layer charging current I_C can be related to the scan rates through Eq. S1:

$$I_C = C_{dl} \times v \qquad \text{(S1)}$$

Thus, plotting the charging currents at a specific potential against various scan rates leads to a straight line with the slope equal to C_{dl}. Subsequently, the EASA value can be obtained by Eq. S2:

$$\text{EASA} = C_{dl} / C_S \qquad \text{(S2)}$$

where C_S is the capacitance measured from ideally smooth, planar surfaces of the catalyst.

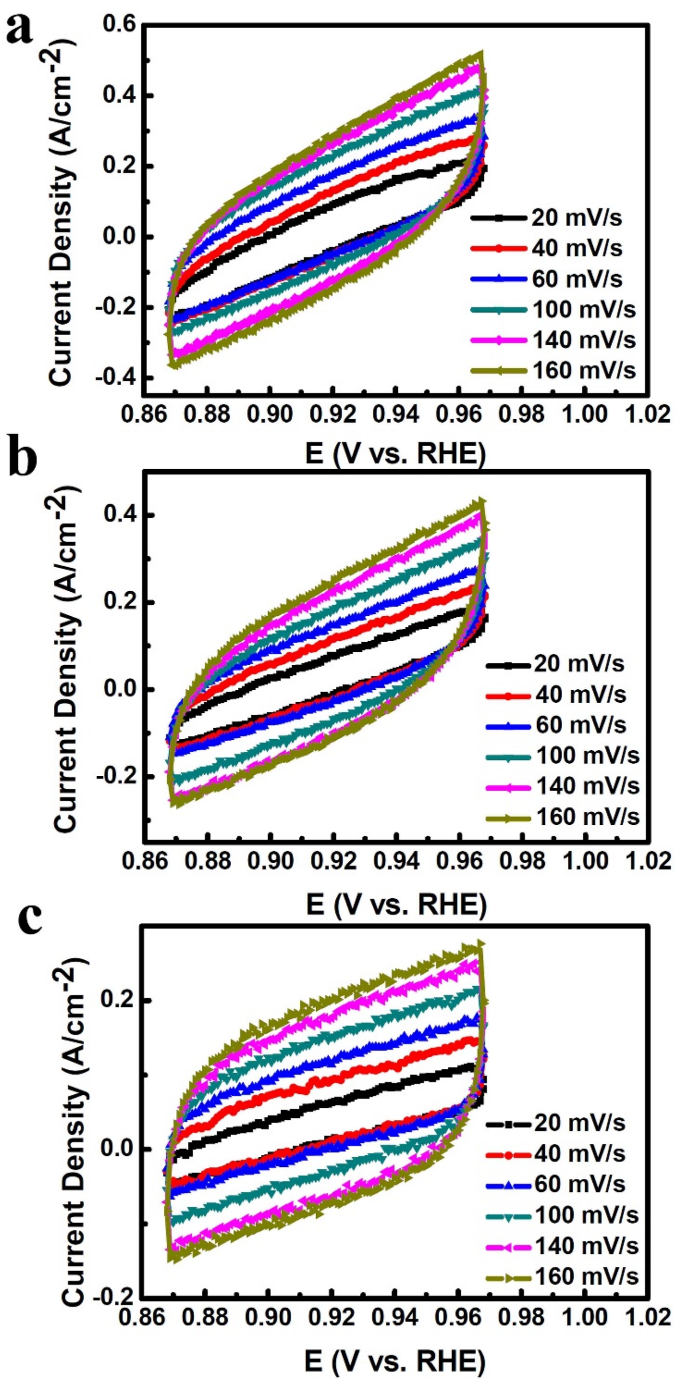

Fig. S9. CV curves of (a) $Co_{5.7}Ni_{2.3}$-POM@FGDY, (b) $Co_{5.7}Ni_{2.3}$-POM and (c) Ni foam in the potential range of 0.86-0.96 V vs RHE at various scan rates (20-160 mV s^{-1}).

9. EIS Nyquist plots

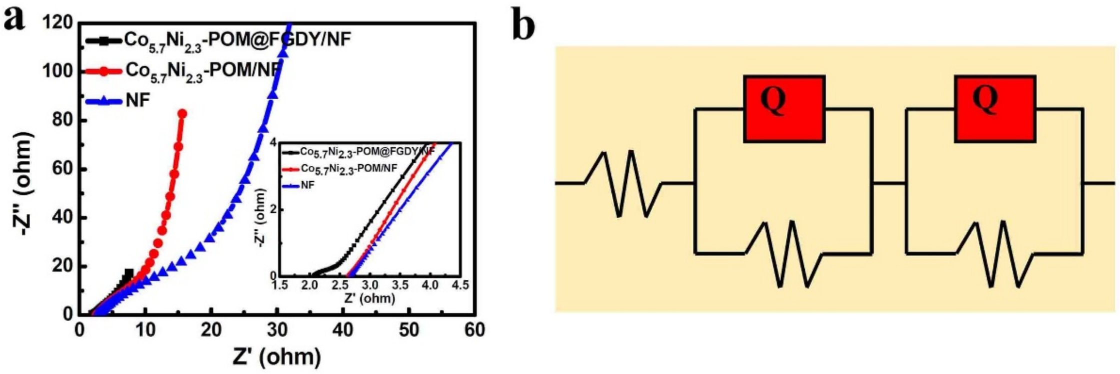

Fig. S10. (a) EIS Nyquist plots of the $Co_{5.7}Ni_{2.3}$-POM@FGDY, $Co_{5.7}Ni_{2.3}$-POM and Ni foam; (b) The circuit equivalent model used for the data fitting.

10. SEM of $Co_{5.7}Ni_{2.3}$-POM@FGDY

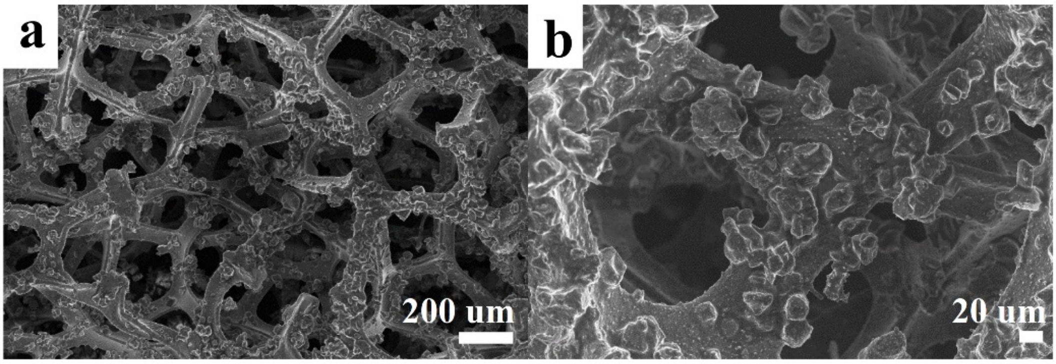

Fig. S11. After 20h OER, (a) the overview SEM image of the $Co_{5.7}Ni_{2.3}$-POM@FGDY electrode; (b) high-magnification SEM image of the CoNi-POM@FGDY.

Table S1. TOF and relevant parameters of nanocomposite electrodes

	$Co_{5.7}Ni_{2.3}$-POM@FGDY	**$Co_{5.7}Ni_{2.3}$-POM**
Q_{redox} in CV [C]	0.01977	0.01393
Moles of active sites [mol cm^{-2}]	1.02×10^{-7}	7.22×10^{-8}
Total number of active sites [cm^{-2}]	6.17×10^{17}	4.35×10^{16}
Current density at $\eta = 375$ mV [mA cm^{-2}]	10.682	5.068
TOF value at $\eta = 375$ mV [s^{-1}]	0.58	0.21

Table S2. Literature survey on potential and Tafel slope of the NiCo-based nanostructures for OER.

Electrocatalysts	**Electrolyte**	***j*** ***[mA cm^{-2}]***	**potential (V *vs* RHE)**	**Tafel slop (mV dec^{-1})**	**References**
$Co_{5.7}Ni_{2.3}$-POM@ FGDY/NF	1.0 M KOH	10 20 50 100 200 300	1.57 1.60 1.63 1.66 1.69 1.71	80	*this work*
Wire-like MoS_2/Fe-$NiCo_2$O4	1.0 M NaOH	10	1.54	42	*2*
$[Co_{6.8}Ni_{1.2}W_{12}O_{42}(OH)_4(H_2O)_8]$	0.1 M KOH	10	1.59	126	*3*
CoO/Co_3O_4	1.0 M KOH	10	1.50	55	*4*
Co_3O_4/N-graphene	1.0 M KOH	10	1.54	67	*5*
CoNi1@C	1.0 M KOH	10	1.57	55	*6*
$NiCo_2O_4@MnO_2$ core-shell	1.0 M KOH	10	1.57	89	*7*

nanoarray					
$NiCo_2O_4$/rGO	0.1 M KOH	10	1.68	53	*8*
$NiCo_2O_4$/NiO nanosheets	1.0 M KOH	10	1.60	61	*9*
CoP/MoP@NC	1.0 M KOH	10	1.50	81	*10*
Fe-$NiCo_2O_4$ nanowire	1.0 M KOH	10	1.58	27	*11*

REFERENCE

1. G. Li, Y. Li, H. Liu, Y. Guo, Y. Li, D. Zhu, Architecture of graphdiyne nanoscale films, *Chem. Commun.*, 2010, **46**, 3256.
2. J. Li, D. Chu, H. Dong, D. R. Baker, R. Jiang, Boosted Oxygen Evolution Reactivity by Igniting Double Exchange Interaction in Spinel Oxides, *J. Am. Chem. Soc.*, 2020, **142**, 50.
3. W. Luo, J. Hu, H. Diao, B. Schewarz, C. Streb. Y. F. Song, Robust Polyoxometalate/Nickel Foam Composite Electrodes for Sustained Electrochemical Oxygen Evolution at High pH, *Angew. Chem. Int. Ed.*, 2017, **56**, 4941.
4. D. He, X. Song, W. Li, C. Tang, J. Liu, Z. Ke, C. Jiang, X. Xiao, Active Electron Density Modulation of Co_3O_4-Based Catalysts Enhances their Oxygen Evolution Performance, *Angew. Chem. Int. Ed.*, 2020, **132**, 6929.
5. Y. Liang, Y. Li, H. Wang, J. Zhou, J. Wang, T. Regier, H. Dai, Co_3O_4 nanocrystals on graphene as a synergistic catalyst for oxygen reduction reaction, *Nat. Mater.*, 2011, **10**, 780.
6. X. Zhang, J. Luo, K. Wan, D. Plessers, B. Sels, J. Song, L. Chen, T. Zhang, P. Tang, J. R. Morante, J. Arbiol, J. Fransaer, From rational design of a new bimetallic MOF family with tunable linkers to OER catalysts, *J. Mater. Chem. A*, 2019, **7**, 1616.
7. H. Xue, H. Yu, Y. Li, K. Deng, Y. Xu, X. Li, H. Wang, L. Wang, Spatially-controlled $NiCo_2O_4$@MnO_2 core-shell nanoarray with hollow $NiCo_2O_4$ cores and MnO_2 flake shells: an efficient catalyst for oxygen evolution reaction, *Nanotechnology*, 2018, **29**, 285401.
8. E. Umeshbabu, G. Rajeshkhanna, P. Justin, G. R. Rao, $NiCo_2O_4$/rGO hybrid nanostructures for efficient electrocatalytic oxygen evolution, *J. Soild State Electrochem.*, 2016, **20**, 2725.
9. C. Mahala, M. Basu, Nanosheets of $NiCo_2O_4$/NiO as Efficient and Stable Electrocatalyst for Oxygen Evolution Reaction**,** *ACS Omega*, 2017, **2**, 7559.
10. Y. J. Tang, H. J. Zhu, L. Z. Dong, A. M. Zhang, S. L. Li, J. Liu, Y. Q. Lan, Solid-phase hot-pressing of POMs-ZIFs precursor and derived phosphide for overall water splitting, *Appl. Catal. B-Environ.*, 2019, **245**, 528.
11. K. L. Yan, X. Shang, Z. Li, B. Dong, X. Li, W. K. Gao, J. C. Chi, Y. M. Chai, C. G. Liu, Ternary mixed metal Fe-doped $NiCo_2O_4$ nanowires as efficient electrocatalysts for oxygen evolution reaction, *Appl. Surface Sci.*, 2017, **416**, 371.